

Electronic Supplementary Information

Synthesis and real time monitoring morphology evolution of luminescent Eu(TCPP) MOF

Xiaohui Wen,^a Yanju Luo,^a Yujia Deng,^c Xiaoliang Zeng,^d Yunfei Tian,^a Juan He^{a*} and Xiandeng Hou^{a,b*}

^a*Analytical & Testing Centre, Sichuan University, Chengdu, Sichuan 610064, China;*

^b*College of Chemistry, Sichuan University, Chengdu, Sichuan 610064, China.*

^c*College of Chemistry and Chemical Engineering, China West Normal University, Nanchong, Sichuan 637009, China*

^d*State Grid Sichuan Electric Power Research Institute, Chengdu, Sichuan 610041, China.*

* To whom correspondence should be addressed. E-mails: [houxd@scu.edu.cn](mailto:houx@scu.edu.cn); hejuan1117@scu.edu.cn

Table S1. Synthesis of Eu(TCPP) MOF with different apparent structures.

	Eu ³⁺ (mmol)	Ligand (mmol)	DMF (mL)	DMA (mL)	Methanol (mL)	Capping agent (mmol)
System 1	0.08	0.02	6	/	/	0.08 (acetic acid)
System 2	0.08	0.02	6	/	/	/
System 3	0.04	0.1	6	/	/	/
System 4	0.02	0.05	6	/	/	/
System 5	0.2	0.02	/	6	/	/
System 6	0.2	0.02	/	6	0.6	/
System 7	0.08	0.02	6	/	/	0.08 (proline)
System 8	0.08	0.02	6	/	/	0.08 (sodium acetate)

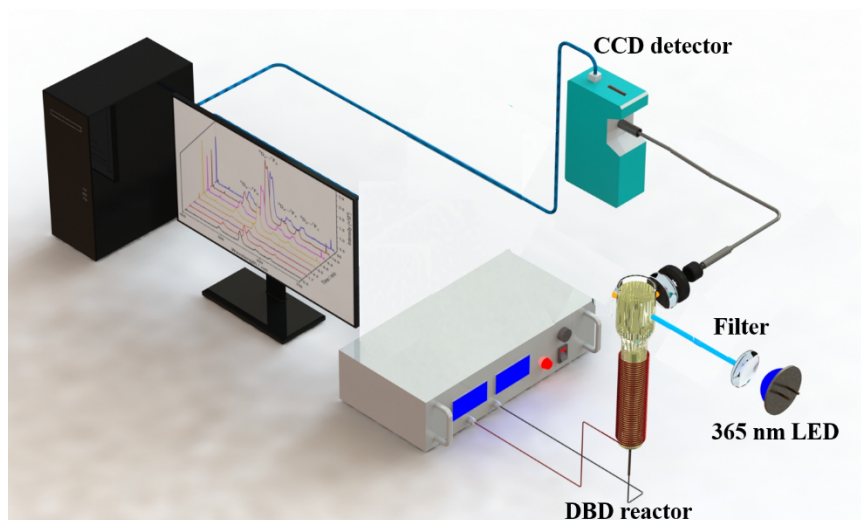


Fig. S1 A device for monitoring the DBD synthesis of Ln-MOFs with time-resolved measurements of luminescence.

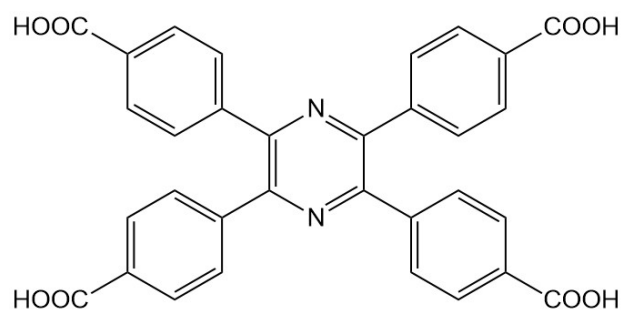


Fig. S2 Molecular structure of 2,3,5,6-tetrakis(4-carboxyphenyl)pyrazine.

1. Results and discussion

1.1 *In situ* monitoring formation of Eu(TCPP)

Preliminary experiments: In our preliminary experiments, Eu(TCPP) MOF was successfully synthesized under the discharge condition of “28 V, 1.30 A” for the DBD, as shown in Fig. S3a. In addition, the monitoring device did not produce background interference (Fig. S3b). To prove this point, let one DBD tube filled with DMF discharge for 60 min, and the background (reflecting light) during the whole reaction remained unchanged (Fig. S3d), indicating the great stabilization of the light source; and another DBD tube filled with TCPP dissolved in DMF solvent discharged for 60 min, and the background (reflecting light) and the optical emission of ligands almost kept unchanged too (Fig. S3c), indicating background interference in the whole reaction was minimal. The red and blue shifts of ligand peak emission spectra are consistent with the red and blue shifts collected by *in situ* monitoring (Fig. S6a and Fig. 1a), indicating the spectral accuracy of the *in situ* monitoring device.

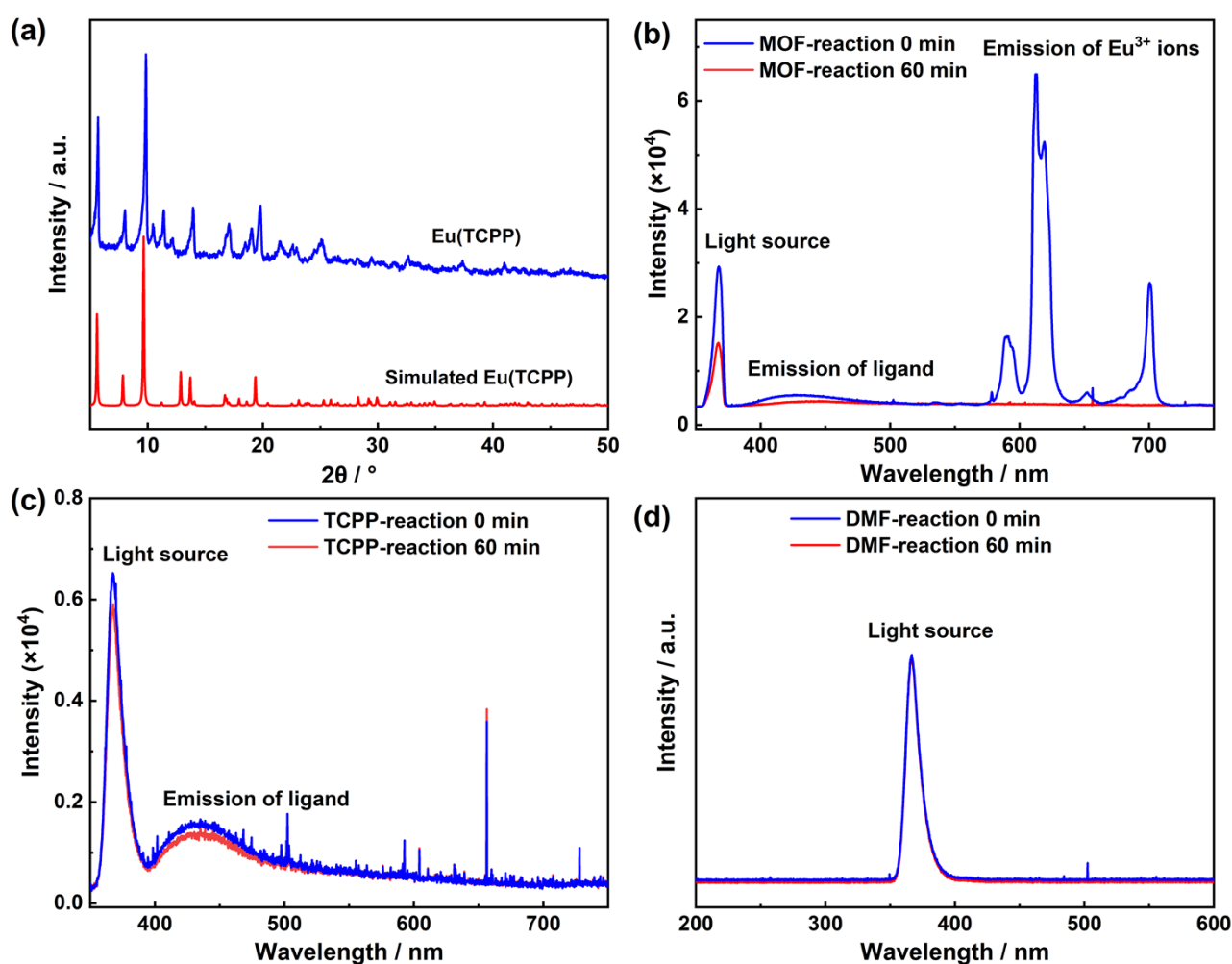


Fig. S3 (a) XRD of Eu(TCPP); (b) Eu^{3+} emission spectra from the mixture of ligand and center ion before and after reaction (MOFs formation); (c) Background spectra of TCPP ligand solution during the discharge; and (d) Background spectra of DMF solution during the discharge.

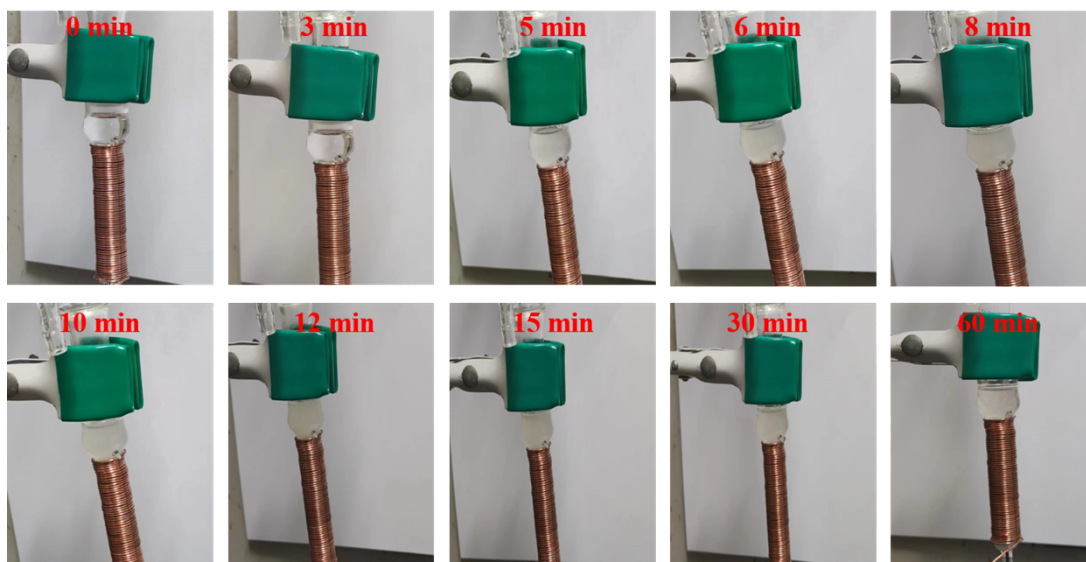


Fig. S4 The images of the solution turbidity change from 0 ~ 60 min during the whole reaction process.

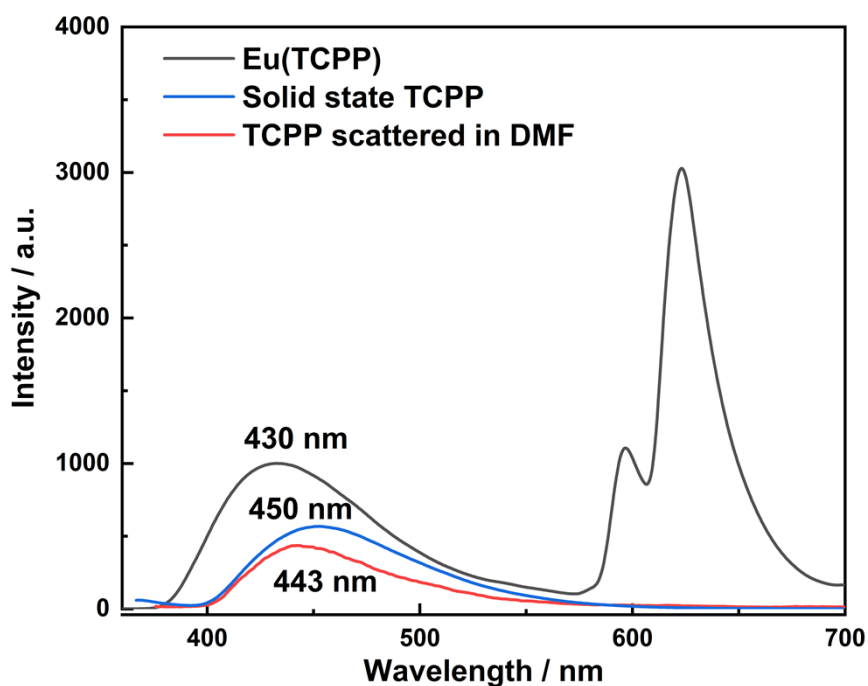


Fig. S5 Fluorescence spectra of Eu(TCPP), solid state TCPP, and TCPP in DMF.

Explanation of ligand redshift: Different from the ligand emission (420 nm) of solid Eu(TCPP) redispersed in DMF (Fig. S6d), the emission of solid Eu(TCPP) was observed to be redshifted to 428 nm (Fig. S6c). Similarly, there was also a significant red shift from 443 nm to 450 nm between the emission peaks of TCPP dispersed in DMF and solid TCPP (red and blue line in Fig. S5). These significant redshifts demonstrated that the greater degree of aggregation in solid materials results in a larger degree of surface-to-surface accumulation between molecules, and this in turn led to the redshift emission.

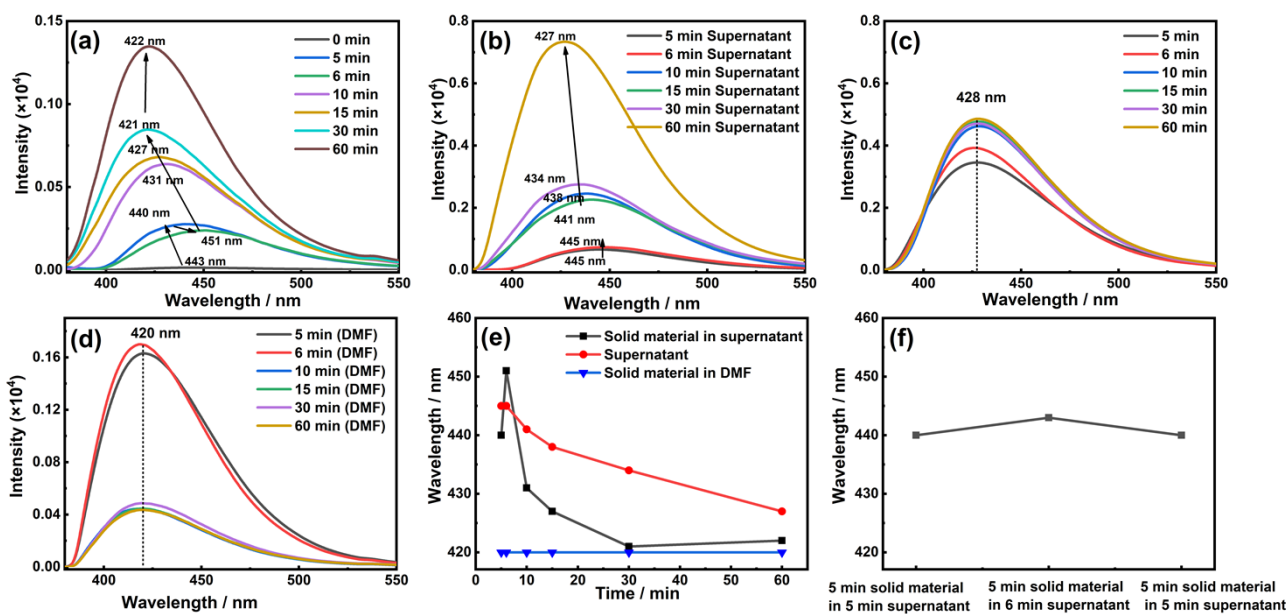


Fig. S6 (a) Fluorescence spectra of the DBD synthesis products at different time periods obtained with *ex situ* F-7000 fluorescence spectrometer. Notation: the samples were ultrasonically mixed prior to the determination; (b) Fluorescence spectra of the supernatant at different time periods; (c) Fluorescence spectra of solid materials at different time periods; (d) Fluorescence spectra of solid materials in DMF at different time periods; (e) Time dependence of the peak emission shift; (f) The peak emission wavelength of 5 min solid material dispersed in 5 min supernatant, then in 6 min supernatant, and finally in 5 min supernatant again.

1.2 *In situ* monitoring change of Eu(TCPP) particle size

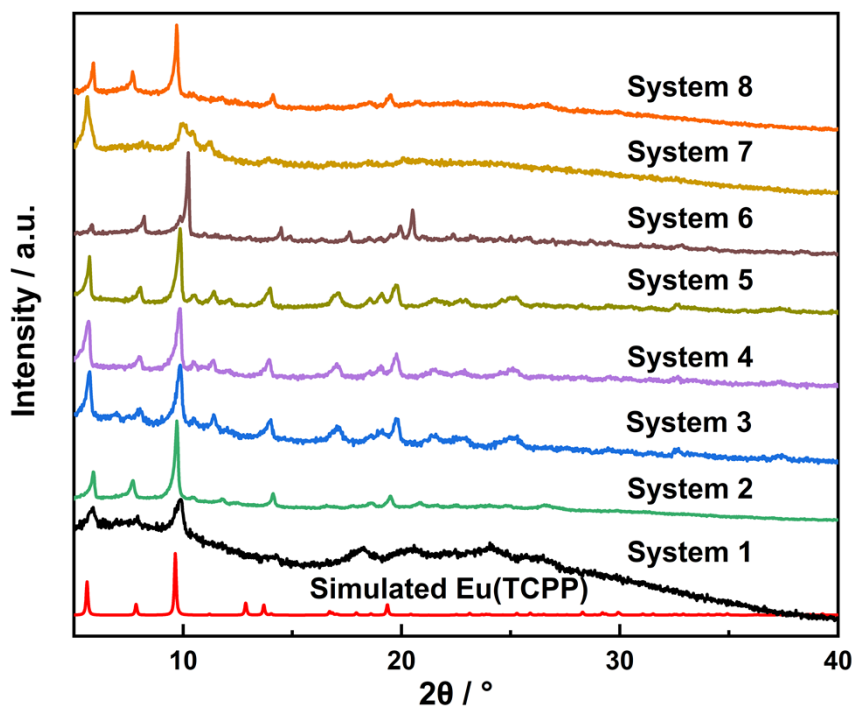


Fig. S7 *Ex situ* XRD measurements of Eu(TCPP) with different morphologies.

Table S2. Eu(TCPP) MOF particle size with different reaction time of system 1~4.

	Induction time (min)	Crystallization time (min)	Settling time (min)	Particle size (μm)
System 1	6.8	7.2	8	12.7
System 2	5.4	6.7	10	7.7
System 3	4.5	5.6	42	4.2
System 4	3.9	3.6	74	1.6

1.3 *In situ* monitoring change of Eu(TCPP) morphology

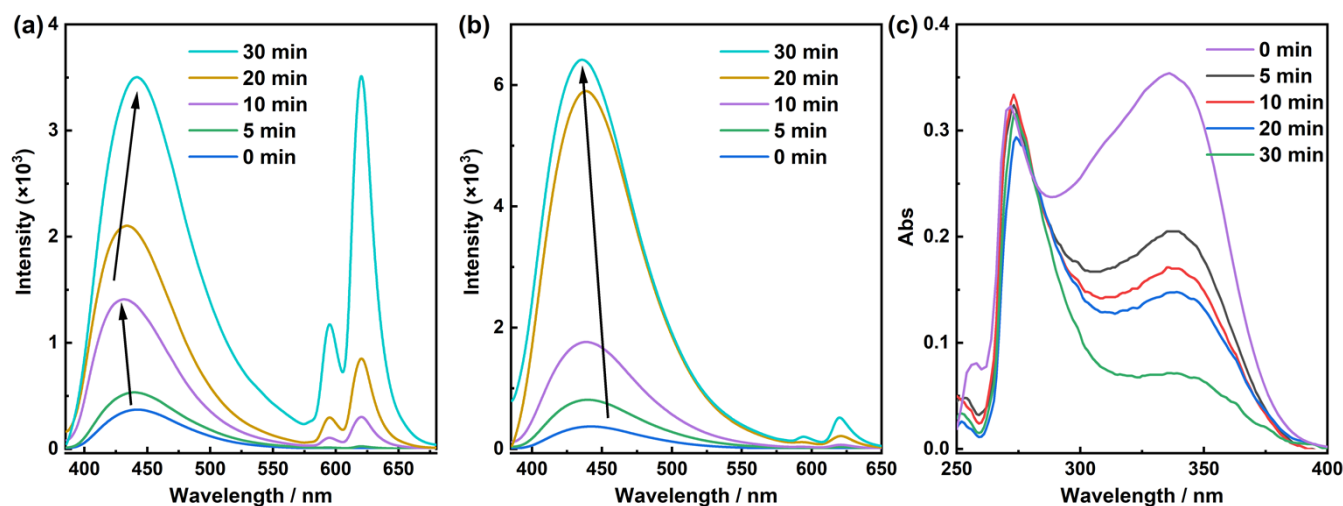


Fig. S8 Fluorescence spectra of MOF materials (a) and its corresponding supernatant (b) from system 5 at different time periods; (c) UV-Vis absorption of the supernatant from system 5 at different time periods (the adsorption at 275 nm was attributed to DMF).

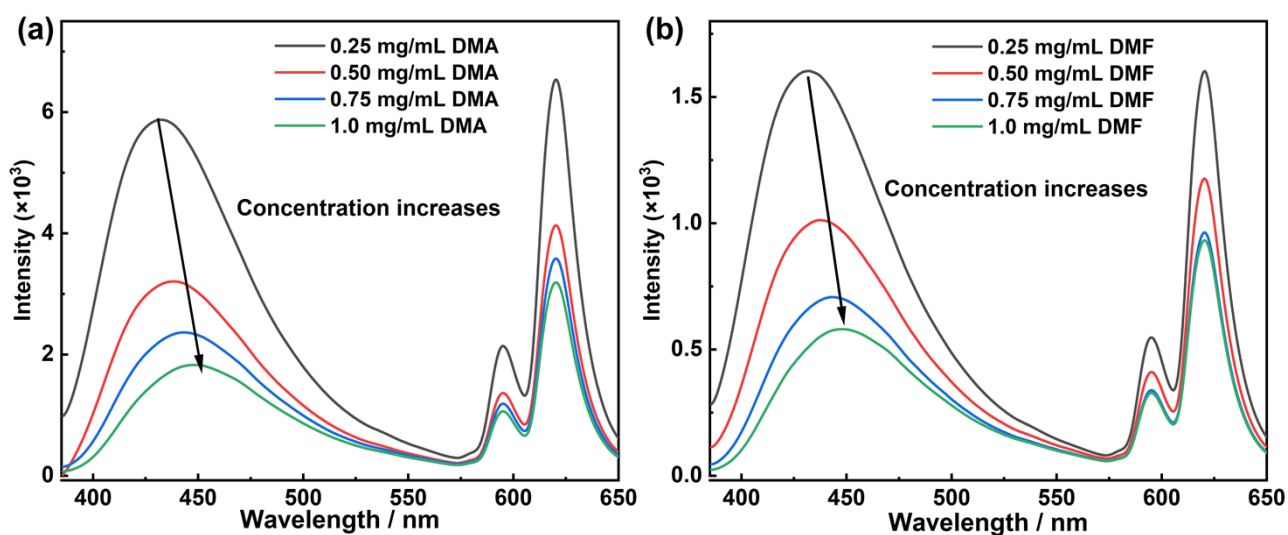


Fig. S9 Fluorescence spectra of Eu(TCPP) MOF from system 5 in DMA solvent (a) and in DMF solvent (b) with different concentrations.

Table S3. The corresponding wavelength emission of ligand in DMA and DMF with different concentrations.

Concentration / mg mL ⁻¹	0.25	0.50	0.75	1.0
Wavelength / nm (DMA)	432	438	443	447
Wavelength / nm (DMF)	432	437	443	448

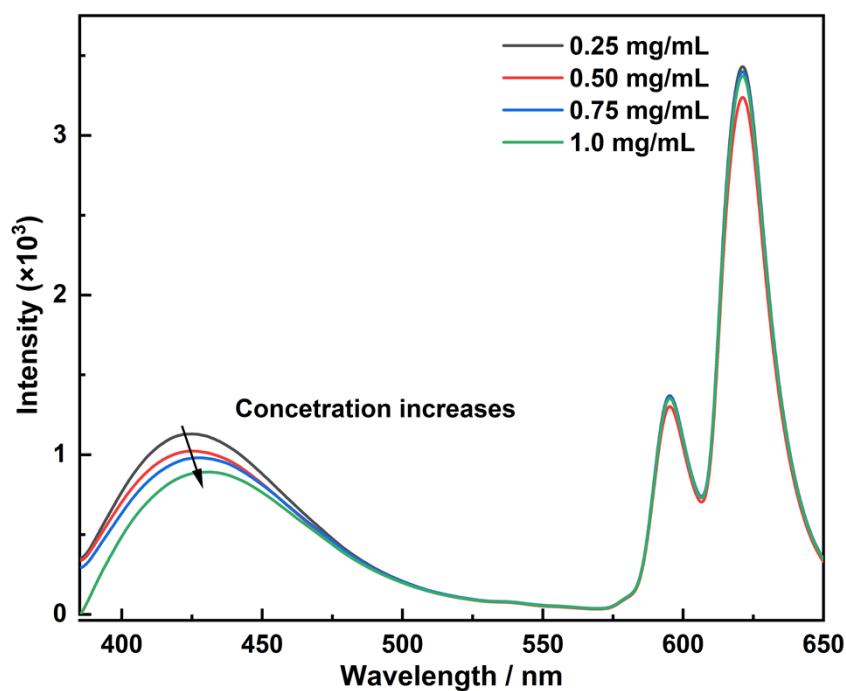


Fig. S10 Fluorescence spectra of Eu(TCPP) MOF from system 2 in DMF solvent with different concentrations.

Table S4. The corresponding wavelength emission of ligand with different concentrations.

Concentration / mg mL ⁻¹	0.25	0.50	0.75	1.0
Wavelength / nm (DMA)	425	425	428	431

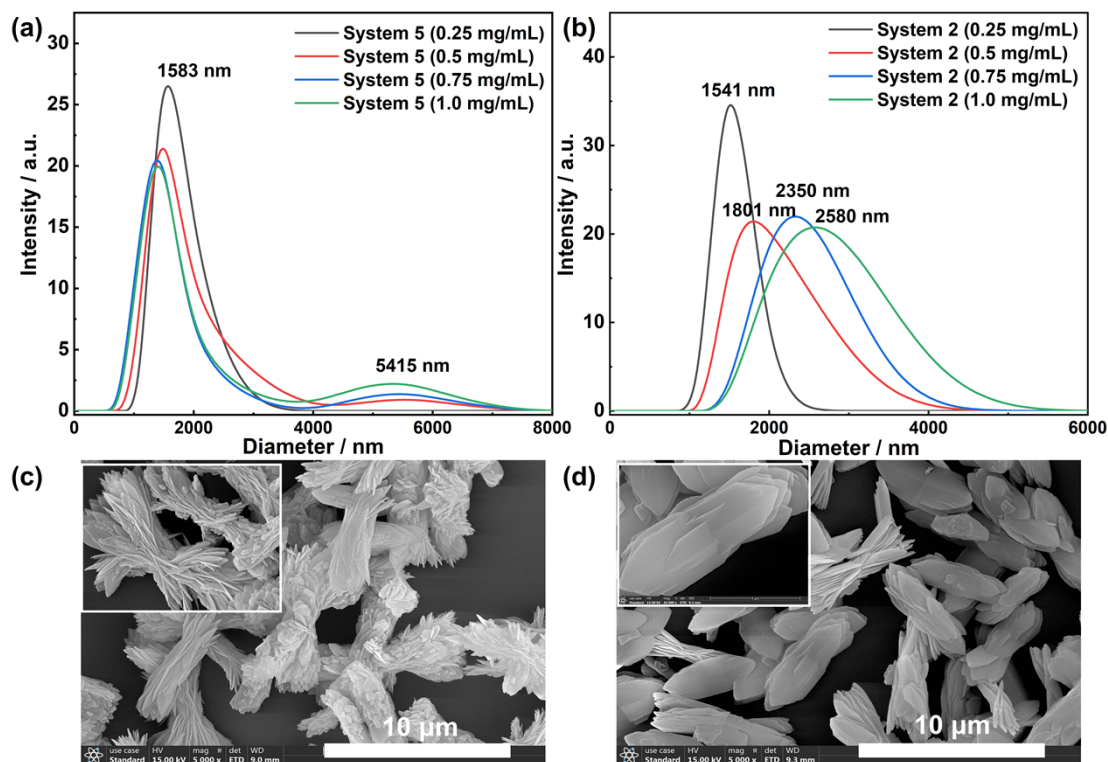


Fig. S11 Laser diffraction particle size distribution curves of Eu(TCPP) from system 5 in DMA (a) and system 2 in DMF (b) with different concentrations; The SEM of Eu(TCPP) from system 5 (c) and system 2 (d).

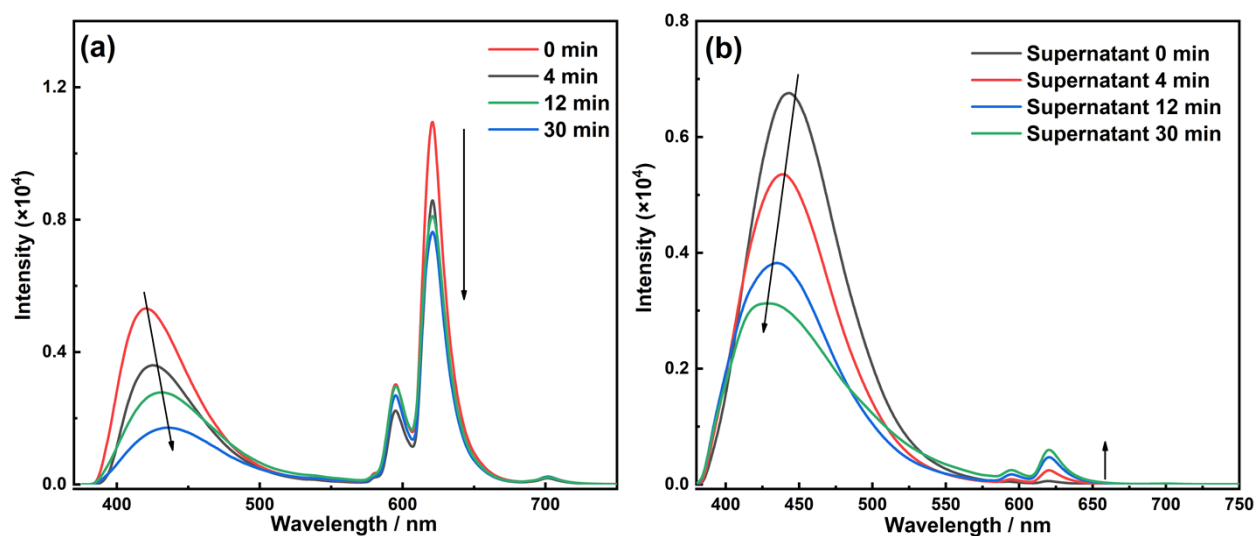


Fig. S12 Fluorescence spectra of Eu-TCPP (a) and supernatant (b) from system 8 at different time periods.

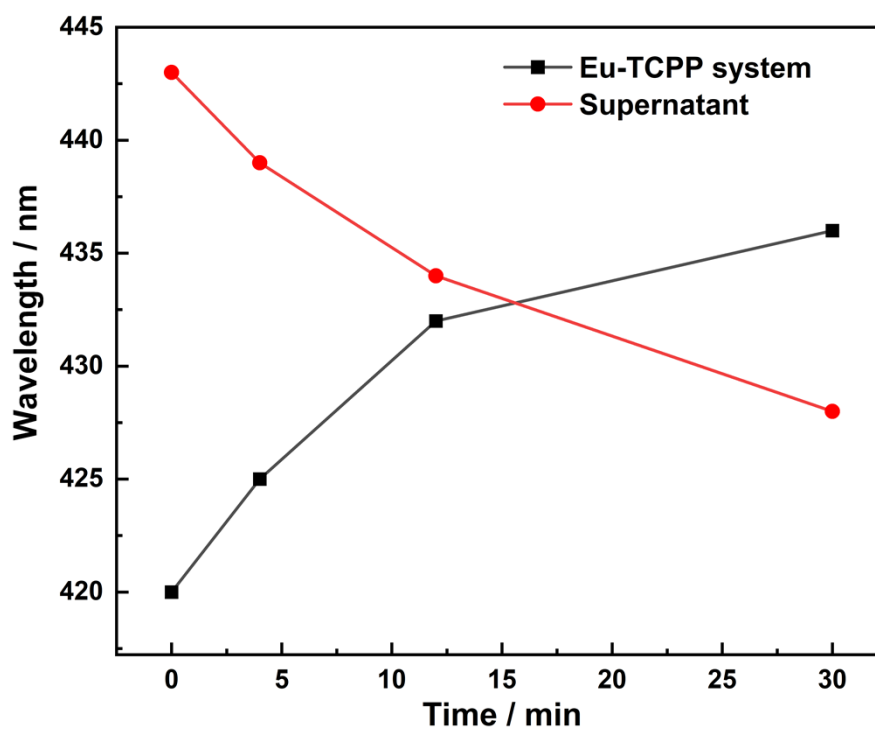


Fig. S13 Wavelength redshift of Eu-TCPP system 8 (black line) and wavelength blueshift of its supernatant (red line) as the reaction proceeded.

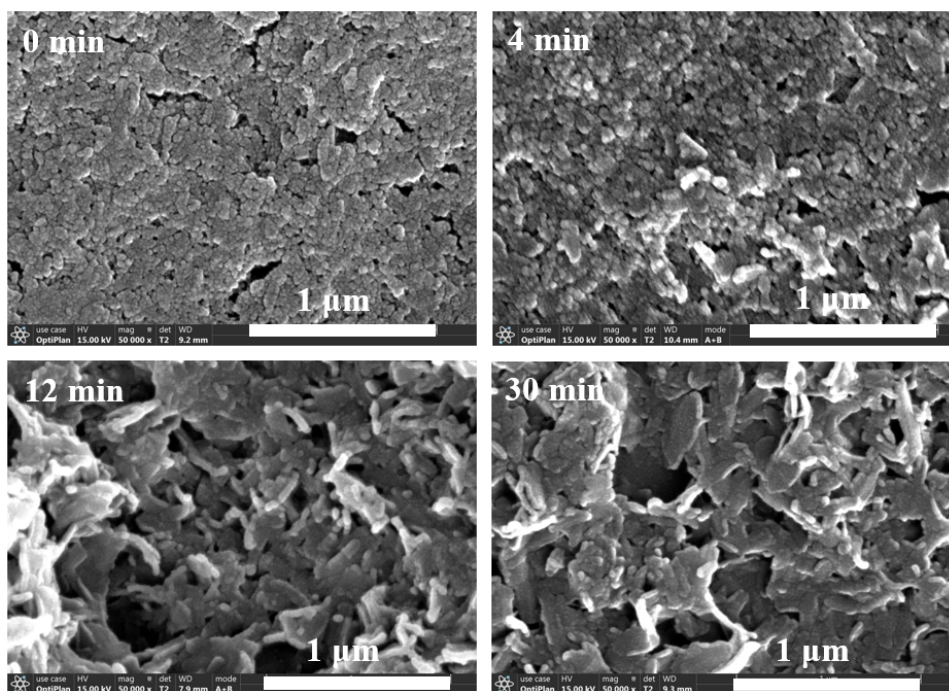


Fig. S14 SEM images of Eu(TCPP) MOF in system 8 with different reaction time.

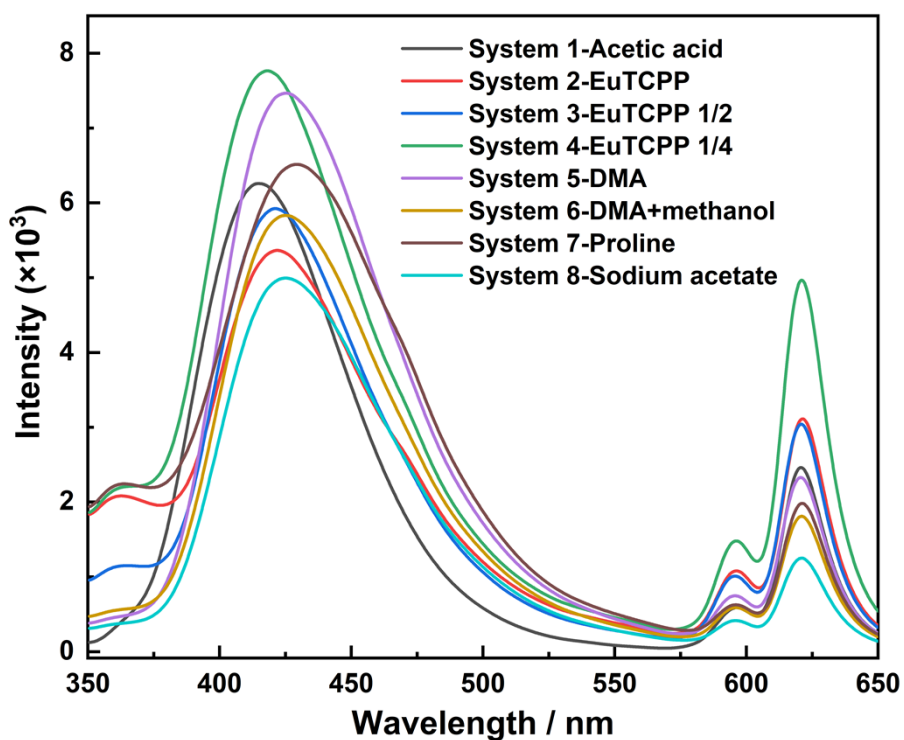


Fig. S15 Fluorescence spectra of solid materials with the same concentration from systems 1 to 8 (0.01 mg).

Table S5. Ligands wavelength of solid Eu(TCPP) obtained by eight types of systems.

System	1	2	3	4	5	6	7	8
Wavelength /nm	418	422	422	418	425	426	429	426

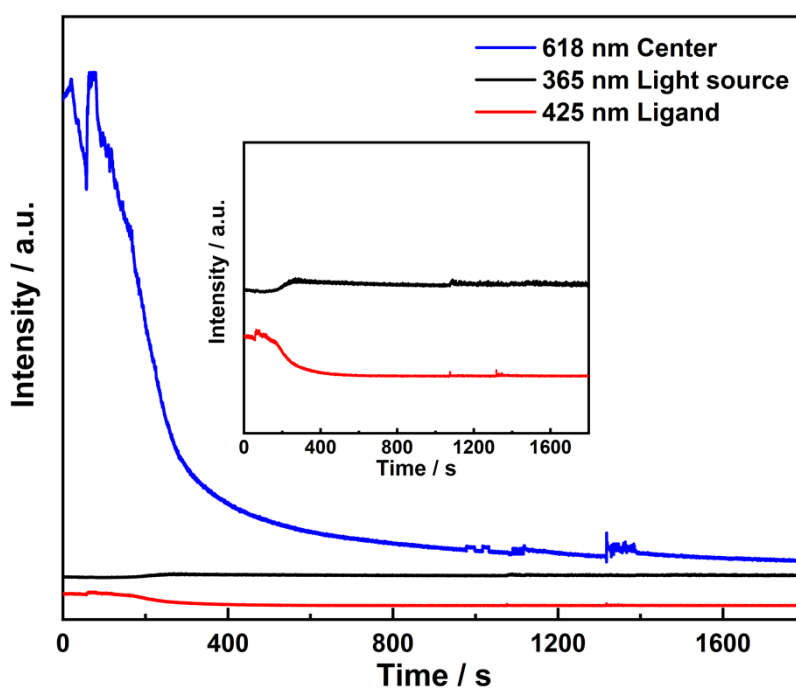


Fig. S16 Intensity variation of the emission from center, ligand and light source for Eu-TCPP system 8 along with the reaction. (inset: enlarged view for the ordinate).

Table S6. Eu(TCPP) MOF particle size and morphology with different reaction time of system 5~8.

	Total time (min)	Particle size (μm)	Product appearance
System 5	43	12.7	rod-like
System 6	27	1	polyhedral sphericity
System 7	22	0.8	fragmentary
System 8	17	0.2	fragmentary

1.4 Analytical application of as-synthesized Eu(TCPP) MOF

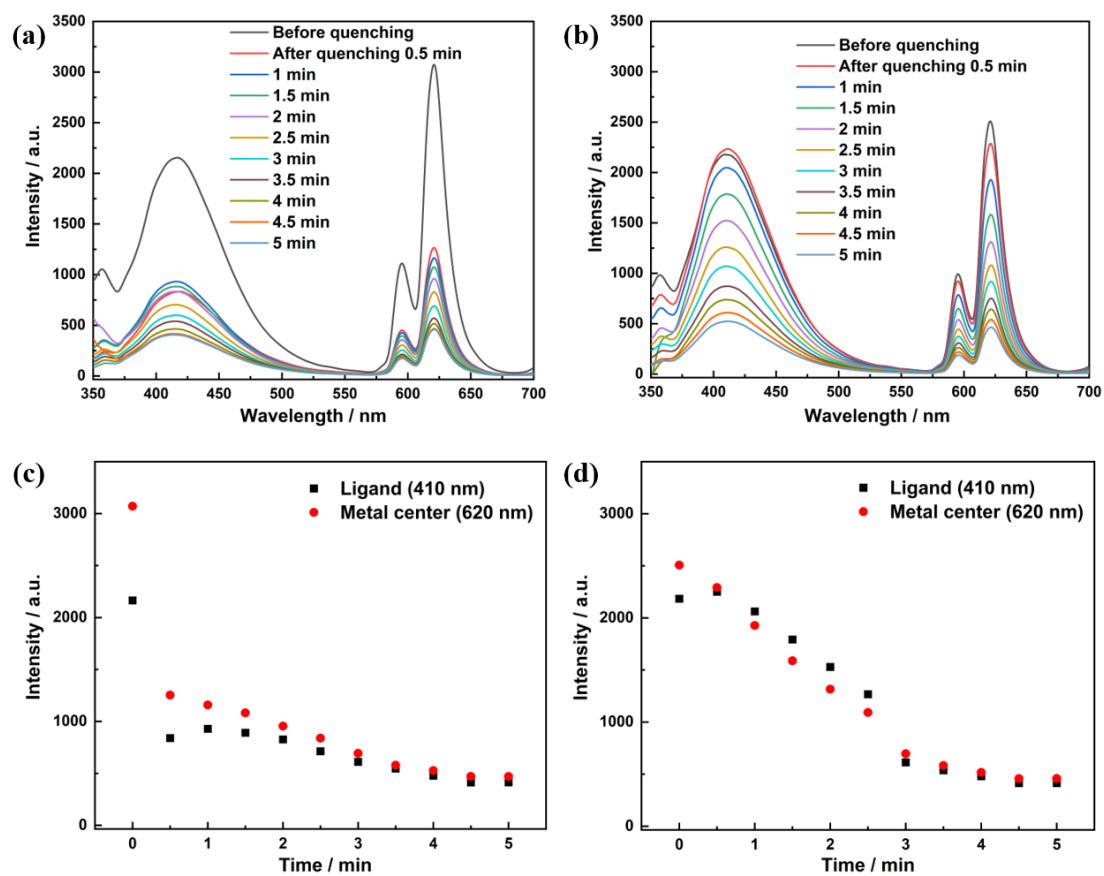


Fig. S17 The response time of Eu(TCPP) MOFs obtained from system 4 (1.6 μm) (a) (c) and system 1 (12.7 μm) (b) (d) to Acac (2500 ppm) under 285 nm excitation.

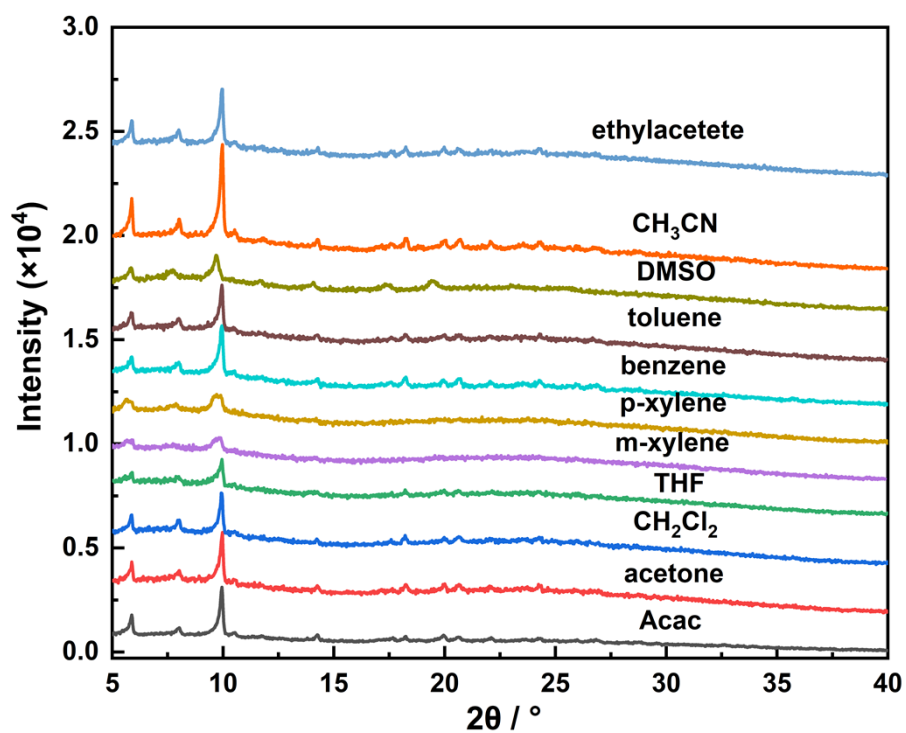


Fig. S18 The PXR D patterns for Eu(TCPP) immersed in common organic solvents for 12 h.

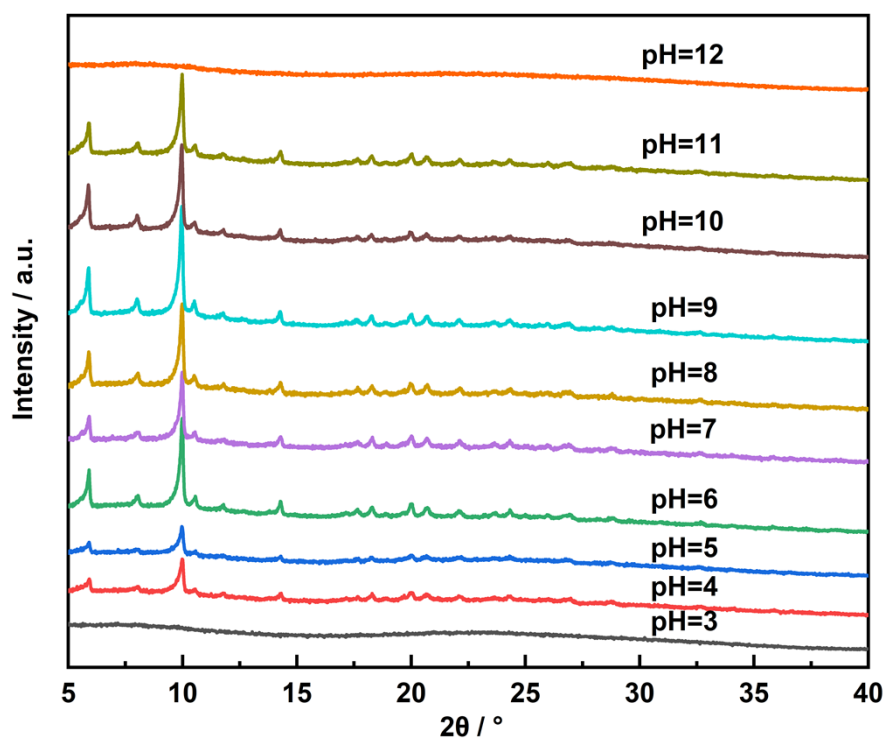


Fig. S19 The PXR D patterns for Eu(TCPP) in solutions with different pH range from 3.0 to 12.0 for 6 h.

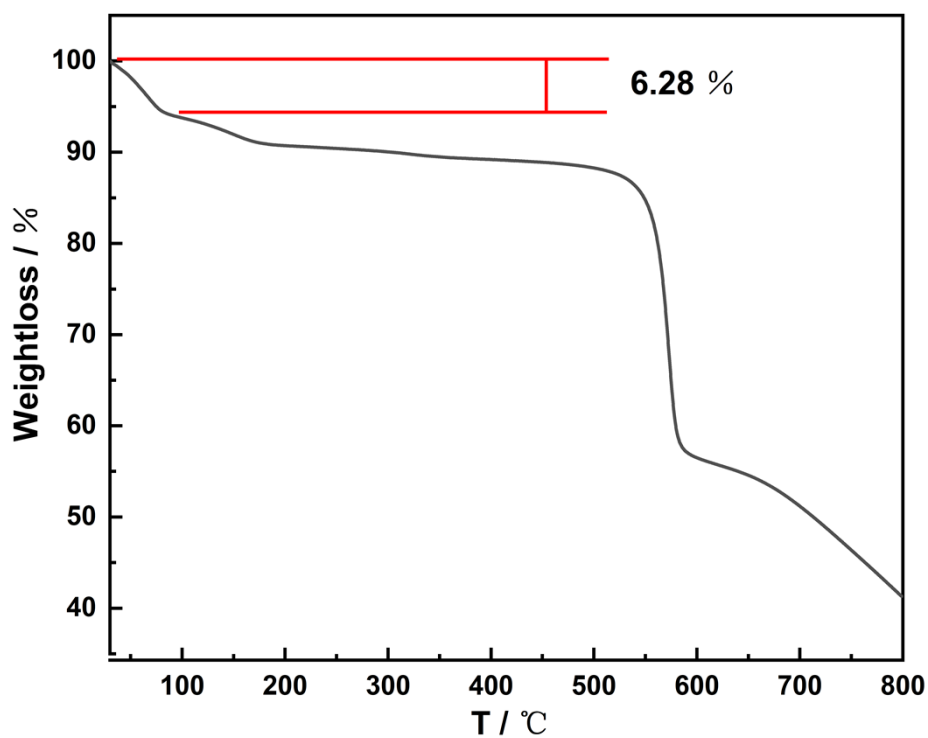


Fig. S20 The TG curve of Eu(TCPP).

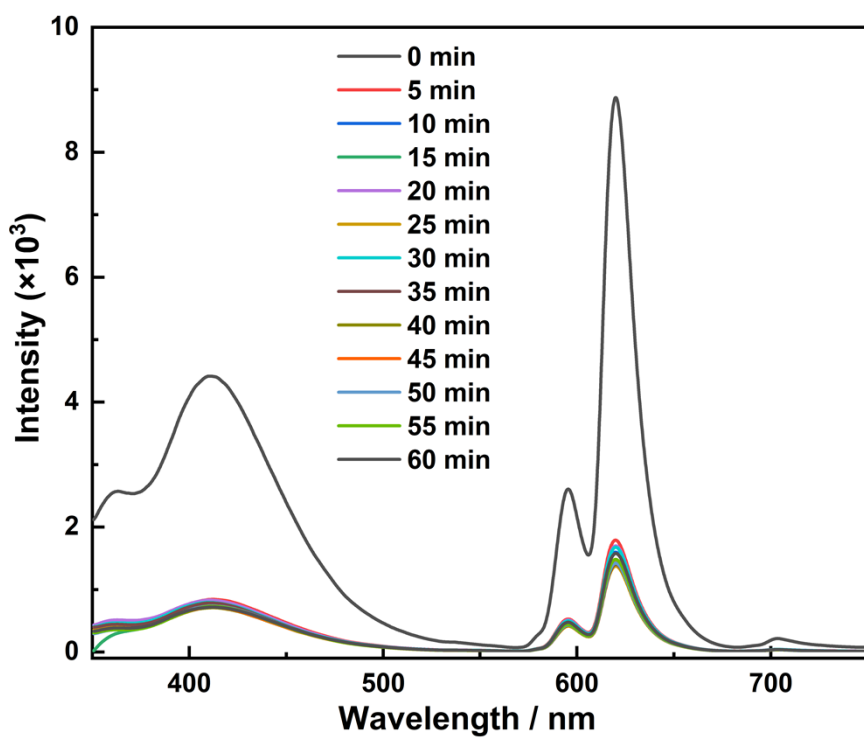


Fig. S21 Dynamic fluorescence spectra of Eu(TCPP) with Acac (2500 ppm) in DMF from 0 to 60 min. The excitation wavelength was 285 nm.

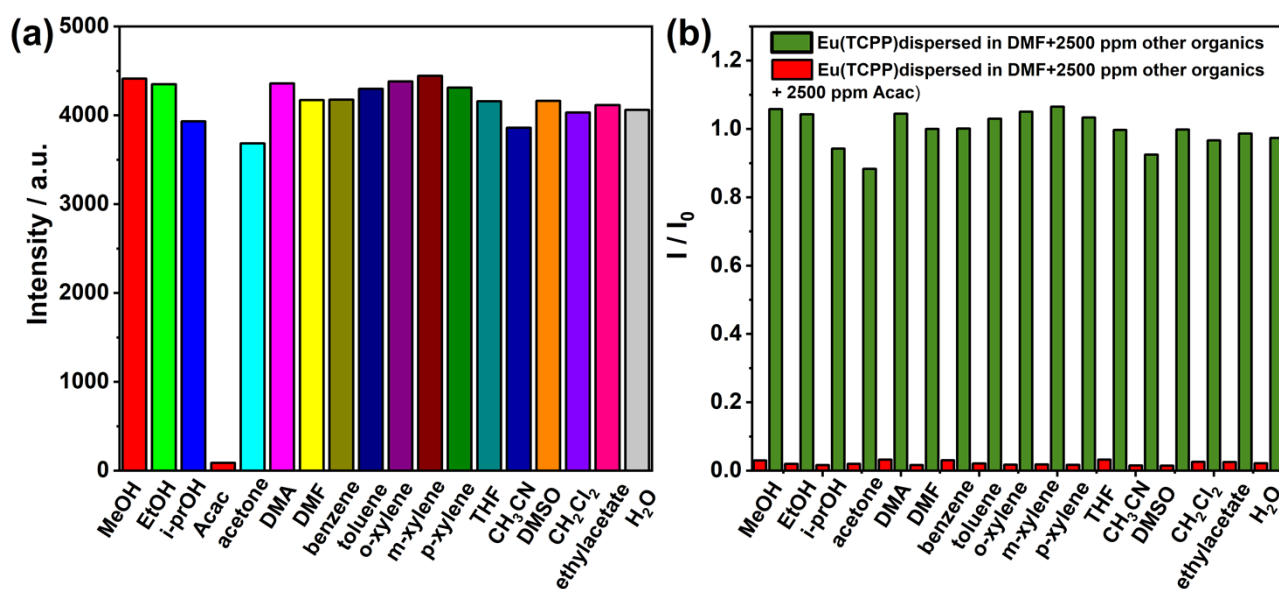


Fig. S22 (a) Fluorescence responses of Eu(TCPP) to Acac and other organics with a concentration of 2500 ppm. (b) Fluorescent responses of Eu(TCPP) to other interferential solvent in the absence (green bar) and presence of Acac (red bar).

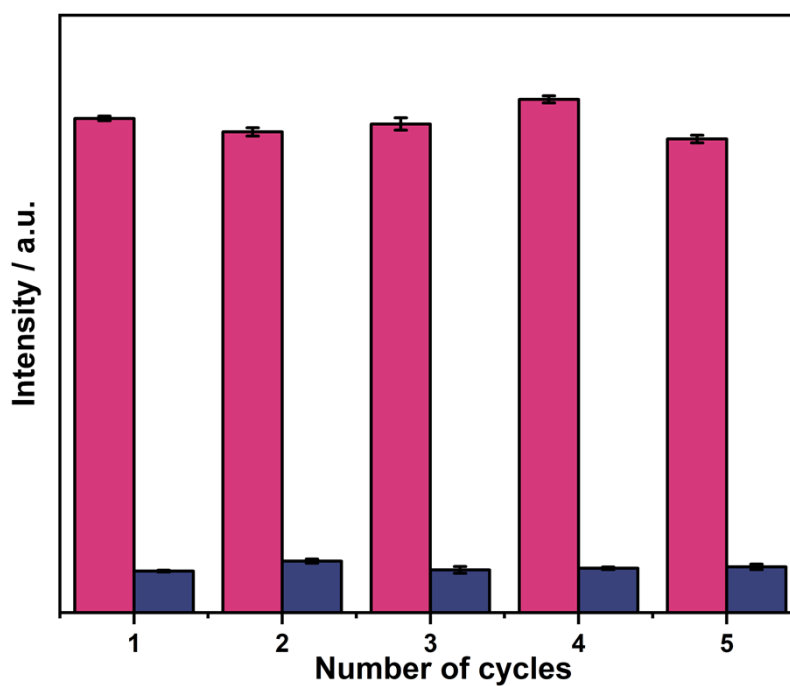


Fig. S23 The luminescence intensity of Eu(TCPP) after five cycles. The intensity is monitored at 620 nm under the excitation wavelength of 285 nm.

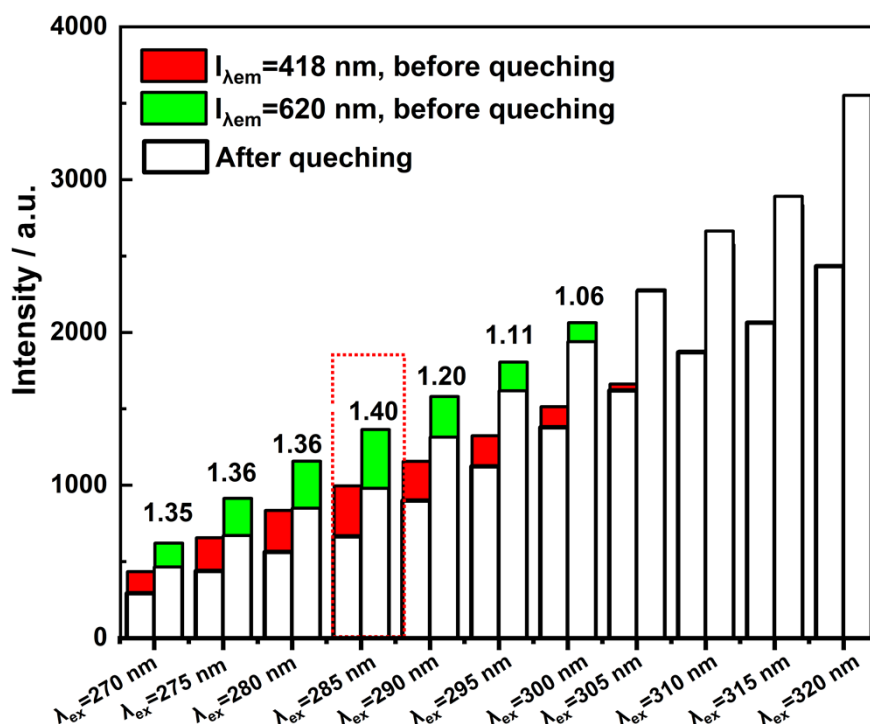


Fig. S24 The emission intensity of Eu(TCPP) with different excitation wavelength. Notation: the ratio is calculated from I_0/I , I_0 : Before quenching; I : After quenching.

Mechanism exploration: The possible quenching mechanism was explored. Firstly, the characteristic PXRD peaks of Eu(TCPP) was retained after being immersed in Acac for 24 h (Fig. S25a), indicating that the luminescence quenching is not caused by the collapse of the framework. Secondly, the bond energies of Eu, O, N, and C in the Eu(TCPP) did not change with or without Acac, demonstrating that there is no strong interaction between the Eu(TCPP) and Acac (Fig. S25c). Thirdly, a distinct UV/Vis absorption of Acac was observed at 260 nm to 310 nm, which overlaps substantially with the excitation spectra of Eu(TCPP) (270 to 400 nm), resulting in an energy competition absorption between Acac and the organic ligand (Fig. S25d). However, the UV/Vis absorption of other common solvents overlaps less with the excitation spectra of Eu(TCPP), indicating Eu(TCPP) has a strong anti-interference capability for sensing Acac. Finally, the fluorescence lifetime of the Eu(TCPP) did not change before and after soaking in Acac, further proving that the detection mechanism was UV coverage (Fig. S25b). Therefore, a possible mechanism of luminescence quenching is owing to the competition absorption by Acac, which resulting in less light absorbed by the ligand and further reduces the efficiency of energy transfer from the ligands to the metal ions in the Eu(TCPP) framework.

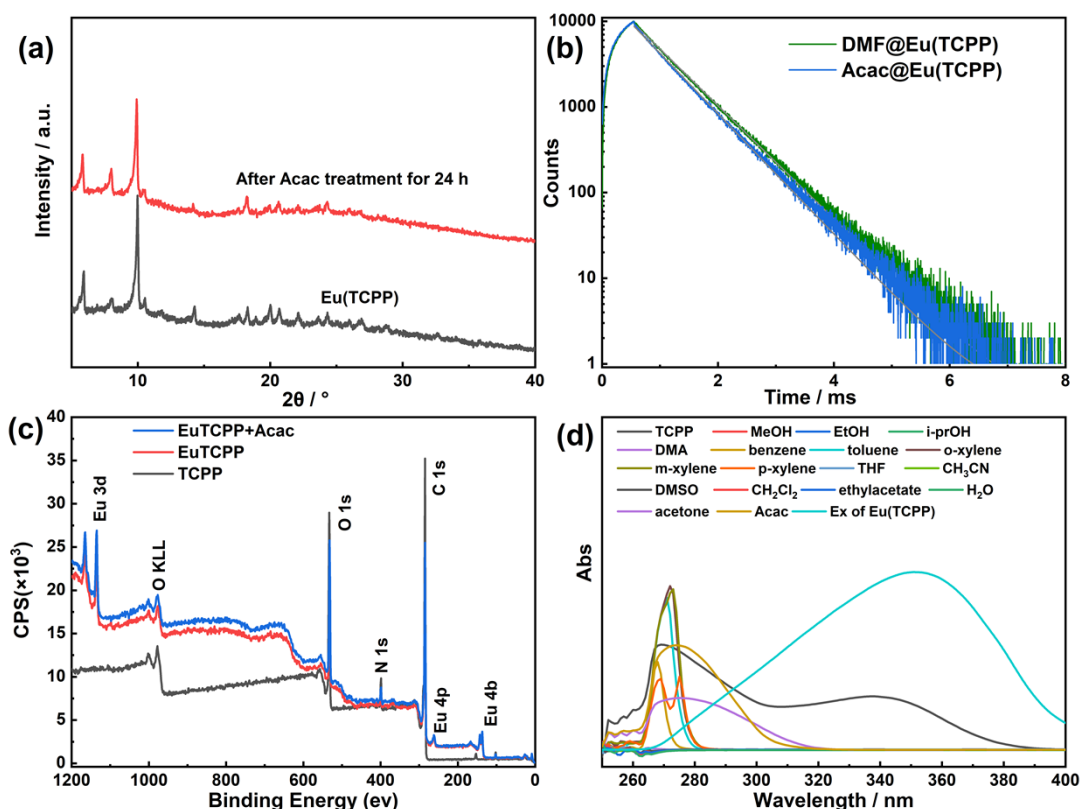


Fig. S25 (a) PXRD patterns of Eu(TCPP), upon the treatment with Acac; (b) Luminescent decay curves of Eu(TCPP), upon the treatment with Acac; (c) XPS spectra of Eu(TCPP), upon the treatment with Acac; (d) The UV-Vis absorption spectra of different solvents in aqueous solution.

Gas sensing device: A device was designed for sensing Acac vapor by placing an Eu(TCPP) film into a cell, followed by adding one droplet (ca. 5 μ L) of Acac into the cell (Fig. 5c). The cell was then capped to form a sealed environment, and the luminescent response of the Eu(TCPP) film for Acac was recorded by a CCD septrometer after 7 min. As shown in Fig. S26, Acac exhibited a significant quenching effect on the characteristic emission at 618 nm of the Eu(TCPP) film, as the Acac evaporized. Therefore, Acac vapor could be effectively sensed with the Eu(TCPP) film, and this provided the foundation for the luminescent sensor for Acac.

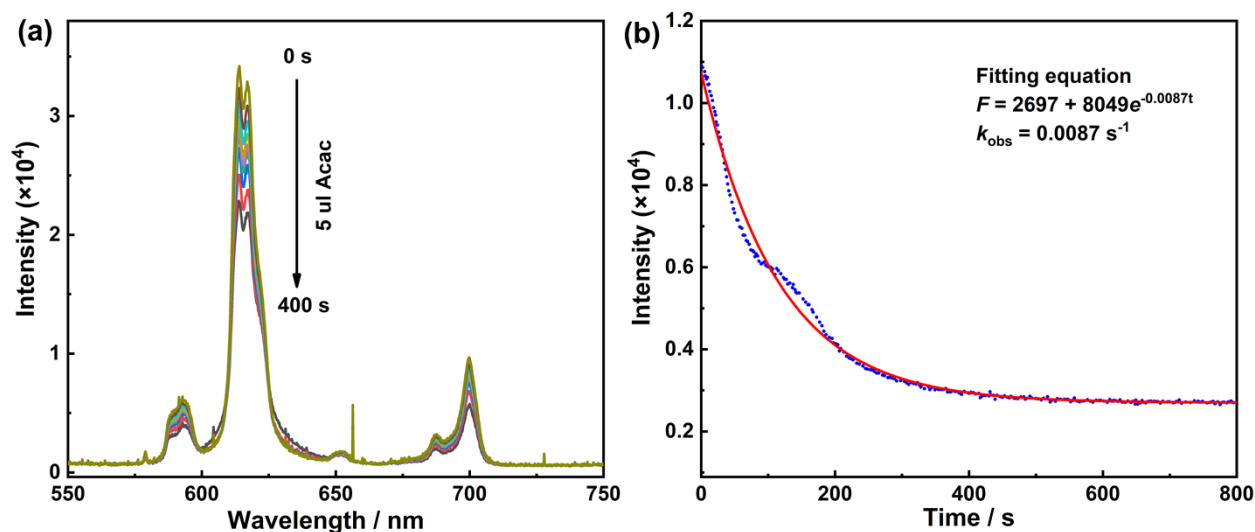


Fig. S26 (a) Time-dependent luminescent spectra of the Eu(TCPP) film in response to 5 μ L Acac vapor; (b) Time-dependent fluorescent decay curves of the Eu(TCPP) film at 618 nm upon the addition of Acac (5 μ L).